IEEE Transactions on Power Electronics

Comprehensive Diagnosis and Tolerance Strategies for Electrical Faults and Sensor Faults in Dual Three-Phase PMSM Drives

Journal:	*IEEE Transactions on Power Electronics*
Manuscript ID	TPEL-Reg-2018-03-0648
Manuscript Type:	Regular Paper
Date Submitted by the Author:	30-Mar-2018
Complete List of Authors:	Wang, Xueqing; Southeast University, School of Electrical Engineering Wang, Zheng; Southeast University, School of Electrical Engineering Xu, Zhixian; Southeast University, School of Electrical Engineering Cheng, Ming; Southeast University, Department of Electrical Engineering Hu, Yihua; University of Liverpool
Keywords:	AC motor drives, Fault diagnosis, Fault tolerance, Pulse width modulated inverters, Torque control

Comprehensive Diagnosis and Tolerance Strategies for Electrical Faults and Sensor Faults in Dual Three-Phase PMSM Drives

***Abstract*—In this paper, fault diagnosis and tolerant control strategies have been studied comprehensively for dual-three phase PMSM drives to improve the reliability. Based on direct torque control (DTC) with space vector modulation (SVM), a series of diagnostic and tolerant control methods have been proposed for five types of faults, namely speed-sensor fault, DC-link voltage-sensor fault, current-sensor fault, open-phase fault and open-switch fault. Firstly, diagnosis and tolerant schemes are proposed for speed-sensor fault by estimating the rotor angle speed with the rotating speed of stator flux. Secondly, diagnosis and tolerant schemes are proposed for DC-link voltage-sensor fault by combining the current model based stator flux observer with the voltage model based stator flux observer. Thirdly, a three-step method is designed to diagnose three types of faults related to current signals, namely current-sensor fault, open-phase fault and open-switch fault simultaneously. A vector space decomposition (VSD) based current estimation method is proposed to achieve fault-tolerant control for the current-sensor fault, and the voltage compensation based fault-tolerant control is presented for both open-phase fault and open-switch fault. The experiments have been taken on a laboratory prototype to verify the effectiveness of the proposed fault diagnosis and tolerance schemes.**

***Index Terms*—Dual three-phase PMSM, fault diagnosis, fault-tolerant control, sensor fault, electrical fault, direct torque control.**

I. INTRODUCTION

Permanent-magnet synchronous motors (PMSMs) for variable speed drives are receiving more and more attention due to their high power density and efficiency. Compared to three-phase motor drives, multiphase motor drives offer advantages of larger power rating, lower torque ripple and better fault tolerance [1-2]. Among various multiphase drives, dual three-phase PMSM drives are attractive, since the three-phase power modules have already been commercialized widely [3]. Nowadays, the reliability issue is a critical attribute of diving systems in many industrial applications such as aerospace, electric vehicles, electric elevator, etc [4-5]. There are three main sources of faults in a PMSM driving system: mechanical, electrical, and sensor faults [6-7]. Mechanical faults are usually associated with rotor, such as rotor bearing fault, bent shaft, air gap eccentricity and rotor misalignment, which can be diagnosed through vibration analysis, infrared recognition and so forth [8]. On the other hand, the control system is supported by feedback signals of speed sensor, voltage sensor in DC-link and phase-current sensors. Failures of these sensors are collectively called sensor faults. The faults in stator and inverters are usually known as electrical faults including open-circuit fault and short-circuit fault. The short-circuit faults are very dangerous and may lead to the abnormal overcurrent problem. So, the power converters are usually equipped with specific hardware

protection circuits or fast fuses to isolate the faulty parts [9-10]. Thus, the short-circuit faults become open-circuit faults. In practice, any fault mentioned above will degrade the system performance, even cause the system breakdown [11-12]. So, it is extremely important for the drive system to possess fault-tolerant capability for these faults, including fault diagnosis and fault tolerance. In this paper, the diagnostic and tolerant methods are presented for speed-sensor fault, voltage-sensor fault, current-sensor fault, open-phase fault and open-switch fault comprehensively.

The mostly common fault diagnostic methods for driving system can be classified into two categories: the model based methods [7, 13-14], and the signal based methods [15-19]. The model based diagnosis relies on the model of electrical machine to estimate the signal. The error between the measured signal and the estimated signal is used as a fault detector. In [7], an adaptive observer is used to diagnose three types of sensor faults by estimating stator currents, rotor fluxes, and rotor resistance. The outputs of this observer are fed to a decision-making unit to find the type and location of the faulty sensor. In [13], a fault detection algorithm has been presented for PMSM motor drives based on an extended Kalman filter. The failure of any sensor in the typical PMSM drives can be detected and isolated to ensure uninterrupted system operation. In [14], a model-based fault diagnostic method is proposed for the voltage-source inverter fed five-phase permanent-magnet motor drives. Both open-switch faults and open-phase faults can be identified by acquiring errors between the measured phase current and the estimated phase current in an ideal model.

On the other hand, the signal based diagnosis is achieved by extracting specific features of faulty signals. In [15], asymmetry between phase currents is used as a detection of current-sensor fault, and the fault in the speed sensor is determined when field and torque components of stator currents are detected not aligned orthogonally. In [16], a parity space approach is used to identify the faults of current sensors and voltage sensors. The fault detection method is robust to parameter variations, but only applicable for sudden change of sensor signal. In [17], the open-phase fault can be detected and localized with good robustness and detection speeds, by using normalized *x*-*y* currents together with a hysteresis band. In [18], the analysis of symmetrical components is utilized to extract the features of open-phase faults in a five-phase permanent magnet assisted synchronous reluctance motor. This method provides the types of faults by analyzing the pattern of magnitude and phase angle changes of the fundamental signal in the symmetrical components logically. In [19], a diagnostic approach is derived from the operating characteristics of the five-phase PMSM under faults conditions. Both open-switch fault and open-phase fault can be identified based on the current patterns on decoupled subspace and other variables derived from the normalized phase currents. Furthermore, in some literatures, the model based diagnosis and signal based diagnosis are adopted simultaneously to identify multi-class faults. For example, in [20], axes transformation is used to detect the faulty sensor of phase current by acquiring specific features of current, and the speed estimation is taken by using the technique based on the model reference adaptive system.

In the aspect of fault-tolerant methods for driving system, sensor faults are usually tolerated by replacing the incorrect feedback signal with the estimated one. In [13], a Luenberger observer is designed to acquire the estimated value of faulty

current sensor by using the current information from the remaining sensors. In [15], the current compensation and speed compensation methods are designed to achieve fault-tolerant control for current sensor and speed sensor by compensating the incorrect feedback value of faulty sensor. In [21], three independent model based observers are proposed to estimate the speed, DC-link voltage, and phase currents of the PMSM after sensor faults. In particular, the speed sensorless observers based on stator flux estimation and high-frequency signal injection are adopted at normal speed and extremely low speed, respectively.

For open-phase faults, fault-tolerant control is usually achieved by using auxiliary circuit or keeping operation with remaining phases [22-24]. For fault-tolerance purpose, a redundant leg is added to connect with the neutral point of three-phase PMSM through a SCR in [22]. The SCR is turned off in normal operation and turned on in open-phase state. In [23], the five-phase induction motor model is built under open-phase fault condition and the complex space vector modulation is reconstructed based on the model with open-phase fault. By this way, the switching table based direct torque control is extended to the fault-tolerant operation. In [24], the fault-tolerant phase currents of six-phase induction motor under open-phase fault are reconstructed with the cost functions of minimum loss and maximum torque respectively. On the other hand, fault-tolerant operations of open-switch faults are usually achieved by using auxiliary circuits, adopting high-reliability converter topologies, and being forced to be open-phase fault condition [25-26]. A complete survey of auxiliary circuits and high-reliability converter topologies for open-switch faults in three-phase voltage source inverters is presented in [25]. In [26], the open-switch faults of T-type three-level inverter fed asymmetric six-phase PMSM drive are tolerated by using the remaining space vectors, and the fault-tolerant control is achieved for open-phase fault by compensating the voltage difference in the faulty phase with remaining healthy phases.

Although the aforementioned studies of fault diagnosis and tolerance have made great efforts for improving the reliability of motor drives, there are still some limits summarized as following: (1) The sensor faults and electrical faults are seldom considered simultaneously. (2) Most of previous works have discussed the fault diagnosis and fault tolerance separately. (3) To the best of authors' knowledge, there is still no research work for fault diagnosis and tolerance of sensor faults in multiphase motor drives. To solve the challenges in the aforementioned limits of fault diagnosis and tolerant methods, a comprehensive study has been developed on fault diagnosis and tolerance schemes for two-level VSI fed dual three-phase PMSM drives in this paper. The contributions of this work are: Firstly, the diagnostic and tolerant methods are investigated comprehensively for five types of faults, namely speed-sensor fault, voltage-sensor fault, current-sensor fault, open-phase fault and open-switch fault in dual three-phase PMSM drives. The different types of faults can be identified accurately and the misdiagnosis can be avoid effectively. Secondly, the proposed fault diagnosis schemes for sensor faults are valid for both sudden error change and gradual error change. Thirdly, current model based stator flux observer is combined with voltage model based stator flux observer to achieve the diagnosis and tolerance of DC-link voltage-sensor fault. Fourthly, a three-step method is proposed to diagnose three types of faults (current-sensor fault , open-phase fault and open-switch fault)

simultaneously. Fifthly, a vector space decomposition (VSD) based current estimation method is proposed to achieve fault-tolerant control of current-sensor fault. It should be noted that no additional hardware is required for the proposed fault-diagnosis and fault-tolerant schemes.

The rest of this paper is organized as following: The configuration and basic control of dual three-phase PMSM motor drives are described in section II. In section III, five types of electrical and sensor faults in dual three-phase PMSM drive are analyzed to extract features in electric drives. Then, the comprehensive, simple, fast and accurate diagnostic and tolerant control schemes are proposed for the five types of faults in section IV. In section V, the effectiveness of the proposed methods for different types of faults are verified by experiments. Finally, the conclusions are drawn in section VI.

II. CONFIGURATION AND CONTROL

Fig. 1 shows the configuration of the six-phase two-level VSI fed dual three-phase PMSM drives. The dual three-phase PMSM has two sets of three-phase windings, which are spatially shifted by 30 electric degrees. Two neutrals of the dual three-phase windings are isolated for eliminating zero-sequence current inherently.

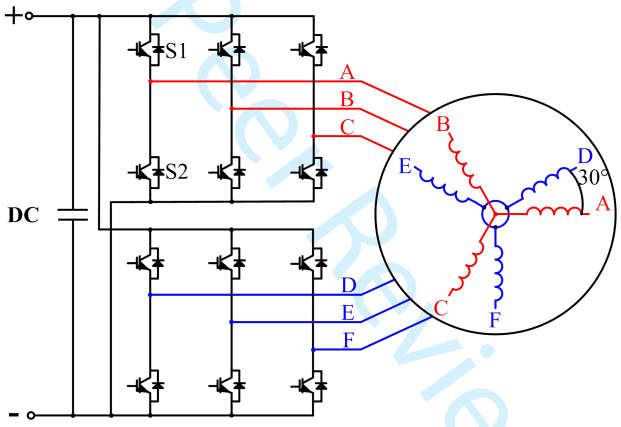

Fig. 1. Configuration of dual three-phase PMSM drive.

The dual three-phase PMSM is a nonlinear high-order system, which makes the analysis and control difficult. By using the vector space decomposition (VSD), the voltage and current space vectors of the dual three-phase PMSM can be decoupled into three two-dimensional orthogonal subspaces: α-β, x-y, and of o_1-o_2 [27]. The components on α-β subspace (torque subspace) comprise the fundamental components related to torque generation. The components on x-y subspace (harmonic subspace) comprise the low order harmonic components which do not participate in torque generation. The components on o_1-o_2 subspace are the zero-sequence components. Eq. (3) shows the decomposition matrix for VSD:

$$\begin{bmatrix} \alpha \\ \beta \\ x \\ y \\ o_1 \\ o_2 \end{bmatrix} = \frac{1}{6} \begin{bmatrix} 2 & -1 & -1 & \sqrt{3} & -\sqrt{3} & 0 \\ 0 & \sqrt{3} & -\sqrt{3} & 1 & 1 & -2 \\ 2 & -1 & -1 & -\sqrt{3} & \sqrt{3} & 0 \\ 0 & -\sqrt{3} & \sqrt{3} & 1 & 1 & -2 \\ 2 & 2 & 2 & 0 & 0 & 0 \\ 0 & 0 & 0 & 2 & 2 & 2 \end{bmatrix} \begin{bmatrix} A \\ B \\ C \\ D \\ E \\ F \end{bmatrix} \quad (1)$$

Fig. 2 shows the control diagram of SVM-DTC scheme for dual three-phase PMSM [28]. The amplitude ψ_s and angle λ_s of the actual stator flux are estimated by the voltage model based flux observer. The amplitude V^* and angle θ_v^* of the reference voltage vector are predicted based on the error of torque angle Δδ and the actual stator flux. It is noted that the low-order current harmonics are easily induced in the dual three-phase motor drives due to relatively small impedance on their harmonic subspaces, and small voltage on *x*-*y* subspace can produce large current harmonics. In order to eliminate the undesirable current harmonics, the reference voltage vector is synthesized through a kind of VSD based SVM: The first step is to utilize inverter voltage vectors to synthesize harmonic-free vectors by forcing the average volt-seconds of voltage vectors on *x*-*y* subspace to be zero. The second step is to use two adjacent harmonic-free vectors to compose the reference voltage vector based on volt-second balancing principle. By dissembling the voltage vector synthesis process into two independent steps, complexity of the SVM scheme could be reduced. It should be noted that the SVM-DTC is developed under stationary frames, and its control of flux and torque are less dependent on synchronization of rotor position. So, the SVM-DTC has higher fault tolerance in terms of position sensor compared to field-oriented control.

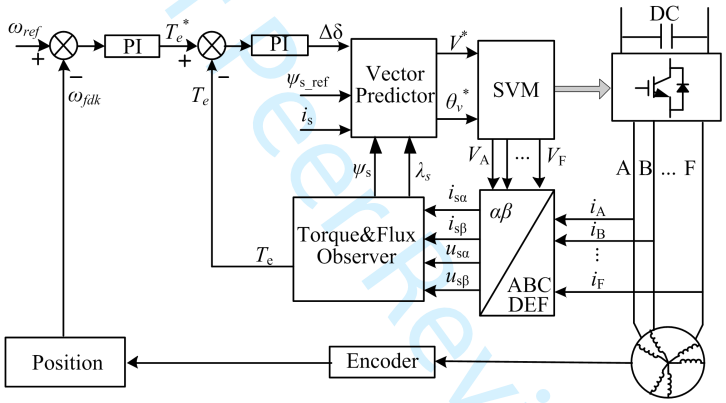

Fig. 2. Control diagram of SVM-DTC for dual three-phase PMSM.

III. FAULT ANALYSIS

Five types of faults in dual three-phase PMSM drive are analyzed in this section, including speed sensor fault, voltage sensor fault, current sensor fault, open-phase fault and the open-switch fault. Different from diagnostic methods for one type of fault, the methods for identifying different types of faults requires avoiding the misdiagnosis. Besides, the complexity of implementation should be reduced. The study of similarities in different faults can be used to classify and simplify the diagnostic process. On the other hand, the study of differences in different faults is used to identify the specific fault precisely and avoid misdiagnosis. Since the probability of simultaneous occurrence of multiple faults is small, only occurrence of single type of fault is involved in the study.

A. Speed-sensor Fault

Speed sensor is usually used to obtain the rotor position and speed for electric drives. Taking the most widely used photoelectric encoder as an example, three pulse signals, namely A B and Z, are generated from the encoder. Signal A and

signal B are orthogonal pulse signals, which provide the position change and the direction of rotation. The speed can be calculated on the basis of position change per unit time. In this paper, the speed is calculated by the position change within a time window of 20ms. The feedback speed is updated in every sampling period, and the diagnostic efficiency will not be affected by the update frequency of speed. The signal Z is the zero-position signal, which is used to correct the position. When signal A or signal B is out of order, both the calculated position and speed of rotor will be incorrect. When the signal Z goes wrong, the accumulative error of position signal caused by outside interference will increase gradually. The worst case of speed-sensor fault is that all the pulse signals disappear. Under this situation, the measured speed will be decreased sharply and maintained as zero. Then, the speed PI controller will be saturated consistently and the actual speed will increase to a maximum value limited by DC-link voltage. It should be noted that the uncontrollable high speed will cause continuous overload and dangerous damage.

B. Voltage-sensor Fault in DC link

The measured DC-link voltage participates in flux estimation and vector prediction in the SVM-DTC scheme for dual three-phase PMSM. According to the faulty severity, the voltage-sensor fault in DC-link can be classified into two cases: The first case is that the error of measured voltage increases suddenly by a large margin, which will cause the breakdown of driving system directly. Under this case, the voltage-sensor fault is required to be rapidly detected in several sampling periods. The second case is that the error of measured voltage changes gradually or varies within a small margin and the driving system can still work for some time. But incorrect feedback voltage of DC-link will cause incorrect estimation of stator flux. Because no fault occurs in the inverter or motor, the voltage on *x*-*y* subspace is still close to zero, which guarantees small current on *x*-*y* subspace.

C. Current-sensor fault

Four phase-current sensors are used to measure the currents of phase-A, phase-B, phase-D and phase-E, in the dual three-phase PMSM driving system in Fig. 1. Owing to isolated neutral points of two three-phase windings, the currents of phase-C and phase-F can be calculated based on Kirchhoff's current law. Similar to voltage-sensor fault, the faults of current sensors can be classified as zero output, incorrect gain, and DC offset. Because the advantage of more phase numbers in dual three-phase PMSM, even the most serious case of current-sensor fault, namely zero output, could not cause the breakdown of driving system. Therefore, the diagnosis of current-sensor fault has no rigorous time limit. By combining Eq. (1) and Kirchhoff's current law, the currents of *x*-axis and *y*-axis can be calculated as:

$$\begin{cases} i_x = \dfrac{1}{6}\left(3i_A - \sqrt{3}i_D - \sqrt{3}i_E\right) \\ i_y = \dfrac{1}{6}\left(-\sqrt{3}i_A - 2\sqrt{3}i_B + 3i_D + 3i_E\right) \end{cases} \tag{2}$$

Since no fault occurs in the inverter or motor, the real current on *x*-*y* subspace is still small under current-sensor fault. But the calculated amplitudes of current components on *x*-*y* subspace are incorrect and large due to incorrect feedback value of faulty current sensor. For example, when the current sensor of phase-A fails, the feedback value of phase-A current i_{A_fdk} can be regarded as the superposition of the real value i_{A_rl} and the error i_{A_err}:

$$i_{A\_fdk} = i_{A\_rl} + i_{A\_err} \tag{3}$$

Since the *x*-axis current and *y*-axis current components are not taken into closed-loop control, both the real currents of *x*-axis and *y*-axis, namely i_{x_rl} and i_{y_rl}, are still zero even under current-sensor fault. Therefore, the feedback values of *x*-axis current and *y*-axis current, namely i_{x_fdk} and i_{y_fdk}, can be approximated as:

$$\begin{cases} i_{x\_fdk} = \dfrac{1}{2} i_{A\_err} + i_{x\_rl} \approx \dfrac{1}{2} i_{A\_err} \\ i_{y\_fdk} = -\dfrac{\sqrt{3}}{2} i_{A\_err} + i_{y\_rl} \approx -\dfrac{\sqrt{3}}{2} i_{A\_err} \end{cases} \tag{4}$$

According to Eq. (4), it is inferred that the trajectory of feedback current on *x*-*y* subspace moves along a straight line with fixed slope. By using the same derivation, different current trajectories of different current-sensor faults can be plotted on *x*-*y* subspace, as shown in Fig. 3. For purpose of analysis and diagnosis, three coordinate systems with 120 degrees of mutual differences, namely x_1-y_1, x_2-y_2 and x_3-y_3, are established on *x*-*y* subspace.

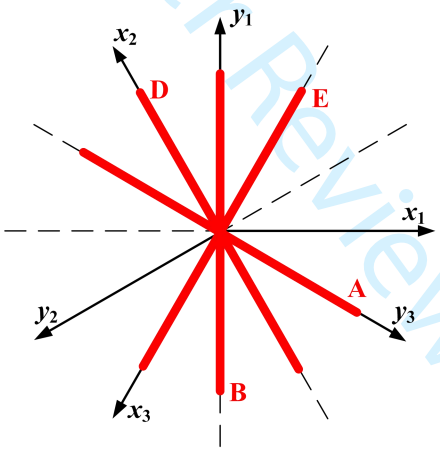

Fig. 3. Current trajectories of different current-sensor faults on *x*-*y* subspace.

D. Open-phase fault

Open-phase fault may occur in the interior or exterior parts of electric machine. Both of the two cases can be regard as a healthy motor with an incorrect terminal voltage in faulty phase. Therefore, the machine model under normal state can be utilized to analyze open-phase fault. The phase voltages of dual three-phase PMSM can be expressed by phase-to-phase voltages as following:

$$\begin{bmatrix} u_A \\ u_B \\ u_C \\ u_D \\ u_E \\ u_F \end{bmatrix} = \frac{1}{3}\begin{bmatrix} 2 & 1 & 1 & 0 & 0 & 0 \\ -1 & 1 & 1 & 0 & 0 & 0 \\ -1 & -2 & 1 & 0 & 0 & 0 \\ 0 & 0 & 0 & 2 & 1 & 1 \\ 0 & 0 & 0 & -1 & 1 & 1 \\ 0 & 0 & 0 & -1 & -2 & 1 \end{bmatrix}\begin{bmatrix} u_{AB} \\ u_{BC} \\ 0 \\ u_{DE} \\ u_{EF} \\ 0 \end{bmatrix} \tag{5}$$

The voltage on *x*-*y* subspaces can be expressed by the line voltages based on Eq. (5) and VSD matrix in Eq. (1).

$$\begin{cases} u_x = \frac{1}{6}\left(2u_{AB} + u_{BC} - \sqrt{3}u_{DE}\right) \\ u_y = \frac{1}{6}\left(-\sqrt{3}u_{BC} + u_{DE} + 2u_{EF}\right) \end{cases} \tag{6}$$

When open-phase fault occurs, abnormal terminal voltage will cause obvious voltage components and current components on *x*-*y* subspace. The faulty phase leads to one or two incorrect line voltages in Eq. (6). For example, when an open-circuit fault occurs in phase-A, only line voltage u_{AB} is abnormal in Eq. (6). when an open-phase fault occurs in phase-B, both u_{AB} and u_{BC} are incorrect in Eq. (6). Under this case, one of the two incorrect line voltages can be eliminated by using Eq. (7).

$$\begin{cases} u_{AB} + u_{BC} + u_{CA} = 0 \\ u_{DE} + u_{EF} + u_{FD} = 0 \end{cases} \tag{7}$$

Taking open-circuit fault in phase-A as an example, the real value of line voltage u_{AB_rl} can be regarded as the superposition of the correct value u_{AB_cot} and the error u_{AB_err}.

$$u_{AB\_rel} = u_{AB\_\mathrm{cot}} + u_{AB\_err} \tag{8}$$

The correct voltages of *x*-axis and *y*-axis, namely u_{x_cot} and u_{y_cot}, are still zero, since the *x*-axis and *y*-axis voltage components are forced to be zero while designing switching strategy. Therefore, the real values of *x*-axis voltage and *y*-axis voltage, namely u_{x_rl} and u_{y_rl} can be estimated from Eq. (6) as following:

$$\begin{cases} u_{x\_rl} = \frac{1}{3}u_{AB\_err} + u_{x\_cot} \approx \frac{1}{3}u_{AB\_err} \\ u_{y\_rl} = u_{y\_cot} \approx 0 \end{cases} \tag{9}$$

Based on Eq. (9), it is inferred that the trajectory of real voltage on *x*-*y* subspace also moves along a straight line with fixed slopes. Therefore, there will be a fixed linear relationship between u_{x_rl} and u_{y_rl}. According to the machine model of *x*-*y* subspace in Eq. (10), the trajectory of real current on *x*-*y* subspace is also a straight line with same slope. By using the same derivation, different current trajectories of different open-phase faults can be plotted on *x*-*y* subspace, as shown in Fig. 4.

$$\begin{cases} u_x = R_S i_x + L_{ls}\frac{d}{dt}i_x \\ u_y = R_S i_y + L_{ls}\frac{d}{dt}i_y \end{cases} \tag{10}$$

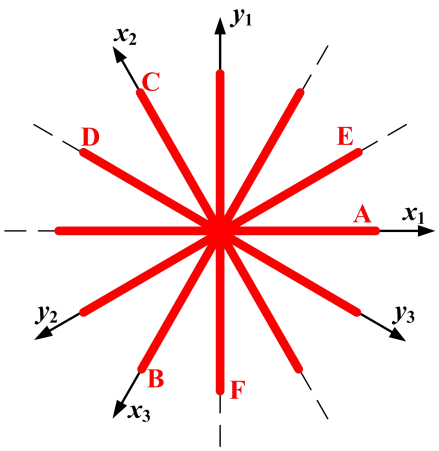

Fig. 4. Current trajectories of different open-phase faults on *x*-*y* subspace.

E. Open-switch Fault

Open-switch fault will cause similar abnormal terminal voltage as the open-phase fault. The difference lies in that the abnormal terminal voltage occurs only when turn-on signal is put on the faulty switch. In other words, the abnormal terminal voltage occurs only in half period of the fundamental wave when single switch falls in open-circuit fault. Therefore, the open-switch fault and the open-phase fault have same slopes of current trajectories on *x*-*y* subspace in Fig. 4. But the current trajectory on *x*-*y* subspace of open-switch fault is only located in one side of the plane. The currents of positive half-wave and negative half-wave in the faulty phase are asymmetric. For example, when the upper switch of phase-A, namely S_{A1} falls in open-circuit fault, the current trajectory on *x*-*y* subspace is located in the right side of the plane, and the current of positive half-wave in faulty phase is almost zero.

IV. Fault Diagnosis and Tolerance Strategies

In order to simplify the diagnostic process, the current-sensor fault, open-phase fault and open-switch fault are distinguished and detected by the same category of diagnostic methods. After that, the corresponding fault tolerant strategies are put into effect accordingly. Fig. 5 shows flowchart of the fault diagnosis process, which will be described in detail as following:

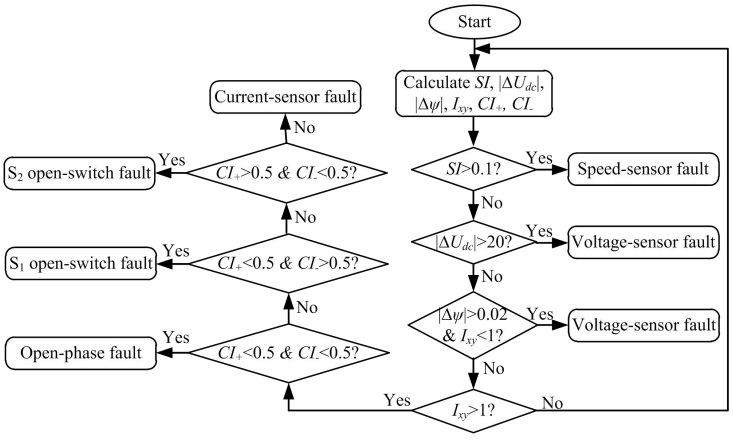

Fig. 5. Flowchart of complete diagnostic process.

A. Speed-sensor Fault

The rotor angular speed can be estimated as [29]:

$$\omega_{et} = \frac{d}{dt}\theta = \frac{d}{dt}(\lambda_s + \delta) = \omega_\psi + \omega_d \approx \omega_\psi \qquad (11)$$

where θ is the rotor angle, λ_s is the angle of stator flux and δ is torque angle. ω_ψ is the speed of stator flux, and ω_d is the differential value of torque angle. Since the value of ω_d is much smaller compared to ω_ψ, it is simple and effective to estimate the rotor angle speed to be the rotating speed of stator flux approximately. When the speed-sensor fault occurs, the error between the feedback speed and the estimated speed will exceed the predetermined threshold, and the speed-sensor fault can be detected accordingly. In this paper, the ratio of absolute error to the rated speed 1000 rpm is defined to be the speed index *SI*, which is compared with the predetermined threshold 0.1 to monitor the speed-sensor fault in real time. Although other faults may disturb accuracy of speed estimation, this diagnosis method is still satisfied to avoid misdiagnosis. So, the speed-sensor fault is judged at first in the flowchart in Fig. 5. After the speed-sensor fault is detected, the incorrect feedback speed will be replaced with the estimated speed ω_{et} to realize fault-tolerant operation.

B. Voltage-sensor Fault in DC link

It has been mentioned in section III-B that the diagnosis of voltage-sensor fault in DC link is required to be classified into two categories: The first case is the condition where the error of measured value by voltage-sensor increases abruptly with a large margin. The second case is the condition where the error of measured voltage changes gradually or varies within a small margin.

Under normal operation, the change of DC-link voltage in one sampling period is limited within a small range, which can be used as the reference value for fault diagnosis of voltage sensor. Therefore, the threshold of diagnosis for the first case of voltage-sensor fault can be designed by adding enough margin to the reference value. For instance, the absolute difference $|\Delta U_{dc}|$ between the measured voltage in previous sampling period and the measured value in present sampling period is smaller than 10V under normal operation. Therefore, the threshold can be set as 20V. When the absolute difference $|\Delta U_{dc}|$ exceeds the predetermined threshold, the voltage-sensor fault can be detected immediately [21]. However, this diagnostic method is designed only for sensor-fault with large measured error. It is not applicable to the second case where the measured error changes gradually or with a small margin.

For detecting the second case of voltage-sensor fault, the stator-flux observer is used. When the second case of voltage-sensor fault occurs, an obvious error will occur between the real one ψ_{rl} and the calculated stator-flux amplitude ψ_{fdk} with voltage model based observer. For instance, if the measured voltage is smaller than the real one, ψ_{fdk} estimated based on voltage mode will be also smaller than ψ_{rl}, and vice versa. Therefore, a current model based stator flux observer is introduced to estimate the real amplitude of stator flux in faulty state, as shown in Fig. 6 [30]. Compared to voltage model

based stator flux observer, the current model based observer is not constrained by voltage signals. Even voltage sensor in DC link falls in fault, the stator flux can be calculated accurately with current model based stator flux observer.

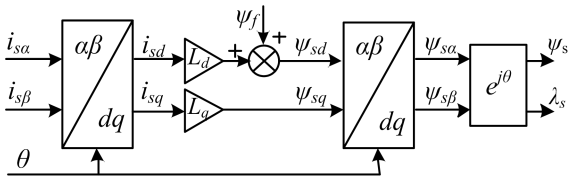

Fig. 6. Calculation of stator flux based on current model.

In this paper, the absolute stator flux error $|\Delta\psi|$ is defined by two stator-flux amplitudes ψ_{fdk} and ψ_{et}, which are acquired from voltage model based observer and current model based observer, respectively. This stator flux error $|\Delta\psi|$ is compared with the predetermined threshold 0.02Wb to distinguish the second case of voltage-sensor fault in real time. In fact, current-sensor fault, open-switch fault and open-phase fault will also cause incorrect stator-flux calculation. Different from them, voltage-sensor fault does not increase the amplitude of current on *x*-*y* subspace. Therefore, the identification of the second case of voltage-sensor fault is dependent on two simultaneous conditions as shown in Fig. 5: The first condition is that the flux error $|\Delta\psi|$ should exceed its threshold. The second one is that the current I_{xy} does not exceed the corresponding threshold value within one fundamental period after the first condition is valid. Thus, it will take one fundamental period to confirm occurrence of the voltage-sensor fault after the abnormal estimation of stator flux is detected. Although the position angel θ is used in the diagnostic method for the second case of voltage-sensor fault, the speed-sensor fault will not be mixed with voltage-sensor fault, since the diagnostic time of the former is much less than that of the later.

Fig. 7 shows a scheme for fault-tolerant control under voltage-sensor fault condition. Because the flux amplitude is positively related to DC-link voltage, a PI controller is employed to generate the compensating voltage U_{cmp}, in such a way that the calculated stator-flux amplitude ψ_{fdk} can track the estimated stator-flux amplitude ψ_{et} stably. U_{dc0} is DC-link voltage measured by voltage-sensor in the last sampling period before voltage-sensor fault is detected. Then, the DC-link voltage U_{dc_et} is estimated by adding U_{cmp} to U_{dc0}. Finally, the incorrect feedback voltage of DC-link U_{dc_fdk} is replaced by the estimated one U_{dc_et} to realize fault-tolerant operation under voltage-sensor faults.

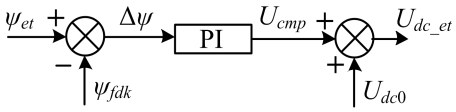

Fig. 7. Fault-tolerant operation for voltage-sensor faults in DC link.

C. Other Types of Faults

Current-sensor fault, open-phase fault and open-switch fault, have similar features of large feedback currents on *x*-*y* subspace, whose trajectories are all straight lines. But different faults in different phases exhibit current trajectories with different slopes, as shown in Fig. 3 and Fig. 4. In addition, the features of phase currents in faulty phases are different. For example, the current-sensor fault of phase-A makes the current on *x*-*y* subspace moves along y_3 axis in Fig. 3. On the other

hand, both the open-phase fault and open-switch fault of phase-A will make the current on *x*-*y* subspace move along x_1 axis, as shown in Fig. 4. The open-phase fault of phase-A forces the phase-A current to be zero. The open-switch fault in S_1 or S_2 of phase-A causes asymmetric phase-A current between positive half-wave and negative one.

A three-step method is proposed to identify the three types of faults in Fig. 5. The first step is to detect the abnormal current amplitude on *x*-*y* subspace, which is calculated as follow:

$$I_{xy} = \sqrt{i_x^2 + i_y^2} \tag{12}$$

In this paper, the current amplitude I_{xy} is compared with the predetermined threshold, 1A in this paper, to judge occurrence of three types of faults in real time. If the current amplitude I_{xy} exceeds its threshold, there must exist one of the three types of faults.

The second step is to identify which axis on x-y subspace the current trajectory moves along. A current comparison method is proposed to identify the direction of current trajectory. At first, the current components of six axes are obtained by phase current as following:

$$\begin{bmatrix} i_{x1} \\ i_{y1} \\ i_{x2} \\ i_{y2} \\ i_{x3} \\ i_{x3} \end{bmatrix} = \frac{1}{6} \begin{bmatrix} 2 & -1 & -1 & \sqrt{3} & -\sqrt{3} & 0 \\ 0 & -\sqrt{3} & \sqrt{3} & 1 & 1 & -2 \\ -1 & -1 & 2 & \sqrt{3} & 0 & -\sqrt{3} \\ -\sqrt{3} & \sqrt{3} & 0 & 1 & -2 & 1 \\ -1 & 2 & -1 & 0 & -\sqrt{3} & \sqrt{3} \\ \sqrt{3} & 0 & -\sqrt{3} & -2 & 1 & 1 \end{bmatrix} \begin{bmatrix} i_A \\ i_B \\ i_C \\ i_D \\ i_E \\ i_F \end{bmatrix} \tag{13}$$

The average absolute value of current component along each axis within one fundamental period is used for judgement. The slope of current trajectory is thus identified by seeking out the axis with smallest current component, since the current component is smallest in the axis perpendicular to the current trajectory. By this way, the axis that current on *x*-*y* subspace moves along is founded and three or four possibilities (Pos1-Pos4) are obtained based on Fig. 3 and Fig. 4, as list in Table I. O_i represents open-circuit fault in phase *i*. S_{i1} and S_{i2} represent open-circuit fault of upper switch and lower switch in phase *i* respectively. CS_i represents current-sensor fault in phase *i*.

TABLE I. CURRENT TRAJECTORY FEATURES

Axis	Pos1	Pos2	Pos3	Pos4
x_1	O_A	S_{A1}	S_{A2}	-
y_1	O_F	S_{F1}	S_{F2}	CS_B
x_2	O_C	S_{C1}	S_{C2}	CS_D
y_2	O_E	S_{E1}	S_{E2}	-
x_3	O_B	S_{B1}	S_{B2}	CS_E
y_3	O_D	S_{D1}	S_{D2}	CS_A

The third step is to further identify the fault type and location based on phase current values. Twelve average absolute currents (I_{A+}, I_{A-}, I_{B+}, I_{B-}, I_{C+}, I_{C-}, I_{D+}, I_{D-}, I_{E+}, I_{E-}, I_{F+} and I_{F-}) of positive parts and negative part in six phases within one fundamental period are calculated after current amplitude I_{xy} exceeds its threshold. The average of all the twelve values is

defined as I_{ave}. Assuming the current trajectory on *x*-*y* subspace moves along y_3 axis, the positive current index CI_{D+} and the negative current index CI_{D-} of phase-D are defined to distinguish the four possibilities. CI_{D+} is defined as the ratio of I_{D+} to I_{ave} and CI_{D-} is defined as the ratio of I_{D-} to I_{ave}. If the open-phase fault occurs in phase-D, both the average absolute currents of positive parts and negative part in phase I_{D+} and I_{D-} are zero, thus the values of CI_{D+} and CI_{D-} are zero. If open-switch fault occurs in S_1 of phase-D, I_{D+} is almost zero where I_{D-} is larger than I_{ave} slightly. Therefore, CI_{D+} is almost zero and CI_{D-} is larger than 1 slightly. Similarly, if open-switch fault occurs in S_2 of phase-D, CI_{D+} is larger than 1 slightly and CI_{D-} is almost zero. On the other hand, if the current-sensor fault occurs in phase-A, both I_{D+} and I_{D-} are close to I_{ave}, and both CI_{D+} and CI_{D-} are close to 1. In order to identify the specific fault precisely, both the thresholds of CI_{D+} and CI_{D-} are set as 0.5. If both CI_{D+} and CI_{D-} are smaller than 0.5, open-circuit fault in phase-D is identified. If CI_{D+} is smaller than 0.5 and CI_{D-} is larger than 0.5, the open-switch fault in S_1 of phase-D is identified. If CI_{D+} is larger than 0.5 and CI_{D-} is smaller than 0.5, the open-switch fault in S_2 of phase-D is identified. If both CI_{D+} and CI_{D-} are larger than 0.5, the current-sensor fault in phase-A is identified. By adopting the proposed three-step method, the current-sensor fault, the open-phase fault and the open-switch fault along the same axis in Table I can be identified accurately within one fundamental period.

For fault-tolerant operation of current-sensor fault, a VSD based current estimation method is proposed. Because no fault occurs in the inverter or motor, the real current on *x*-*y* subspace is still close to zero. Therefore, the relationship can be obtained by approximating the current on *x*-*y* subspace as zero in Eq. (2):

$$\begin{cases} \left(3i_A - \sqrt{3}i_D - \sqrt{3}i_E\right) \approx 0 \\ \left(-\sqrt{3}i_A - 2\sqrt{3}i_B + 3i_D + 3i_E\right) \approx 0 \end{cases} \tag{14}$$

Thus, the current of faulty phase can be estimated based on Eq. (14). For current-sensor faults in phase A, D and E, the reconstruction of current in faulty phase can be developed by using the two equations in Eq. (14) together. Taking current-sensor fault in phase-A as an example, the final estimation value of phase-A current is obtained as:

$$i_{A\_et} = 0.5 \times \frac{\sqrt{3}}{3}\left(i_D + i_E\right) + 0.5 \times \left(-2i_B + \sqrt{3}i_D + \sqrt{3}i_E\right) \tag{15}$$

The incorrect phase current of faulty current-sensor is replaced by the estimated one. For current-sensor fault in phase B, the phase current can be reconstructed by the using second equation of Eq. (14). In practice, the reconstructed phase currents can replace the incorrect values gradually from 0 to 100% within one fundamental period in order to avoid large disturbance in control loop.

For fault-tolerant operation of open-switch fault, the remaining healthy switch of the faulty leg can hardly be used. The total faulty leg must be removed. Therefore, the open-switch fault and the open-phase fault usually adopt the same fault-tolerant control scheme. A voltage compensation based fault-tolerant control is adopted for the open-phase fault [26]. The control structure and the switching strategy of SVM-DTC are unchanged with the proposed fault tolerant control scheme. But a specific voltage change resulting from the faulty phase must be compensated by the remaining healthy phases. For

example, if open-circuit fault occurs in phase-A, there will be a voltage difference between the terminal voltage of phase-A under normal condition and the terminal voltage of phase-A under open-phase fault condition. In order to achieve the same stator flux under faulty operation, the voltage references of α axis and β axis are compensated by Δu_α and Δu_β, respectively, which are expressed in Eq. (16).

$$\begin{cases} \Delta u_\alpha = \dfrac{\sqrt{3}}{6}[R_s(i_D - i_E) + L_{ls}\dfrac{d}{dt}(i_D - i_E)] \\ \Delta u_\beta = 0 \end{cases} \tag{16}$$

V. Experimental Verification

The experiments are carried out on a laboratory prototype to verify the effectiveness of the proposed fault diagnosis and tolerance schemes for the six-phase dual three-phase PMSM drive. In the experiments, the algorithms of diagnosis and control and generation of PWM signals are implemented by DSP controller (TMS-F28335). A permanent-magnet synchronous generator is coupled to the dual three-phase PMSM to act as the load. The key parameters of the dual three-phase PMSM drive system are shown in Table II.

TABLE II. Parameters of Experimental Setup

Name	***Value***
Pole pair number	3
q-axis inductance	6.21 mH
d-axis inductance	6.21 mH
PM flux (amplitude)	0.2 Wb
Resistor	0.21 Ω
DC link capacitor	1000 uF
Rated speed	1000 rpm
Rated load torque	10 Nm

In order to express the diagnostic results on the scope clearly, a two-dimension table is formed as the indicators of different fault types as shown in Table III. FL1 and FL2 represent the values of two scope signals. According to the values of Signal values of FL1 and FL2, the fault types can be determined by searching the look-up table in Table III. The symbol of NO in Table III represents no occurrence of fault. The symbol of SS represents speed sensor fault, and the symbol of VS represents voltage sensor fault.

TABLE III. Flag of Diagnostic Results

		FL1						
		0	1	2	3	4	5	6
FL2	0	NO	CS_A	CS_B	-	CS_D	CS_E	-
	1	SS	S_{A1}	S_{B1}	S_{C1}	S_{D1}	S_{E1}	S_{F1}
	2	VS	S_{A2}	S_{B2}	S_{C2}	S_{D2}	S_{E2}	S_{F2}
	3	-	O_A	O_B	O_C	O_D	O_E	O_F

Fig. 8 presents the dynamic performance of SVM-DTC for the dual three-phase PMSM drive without fault. The given speed is switched between 200rpm and 1000rpm. It is obvious that the speed index *SI*, absolute flux error $|\Delta\psi|$ and current amplitude on *x*-*y* subspace I_{xy} are below their corresponding threshold values 0.1, 1A and 0.02Wb, indicating no fault occurs during both transient and steady states.

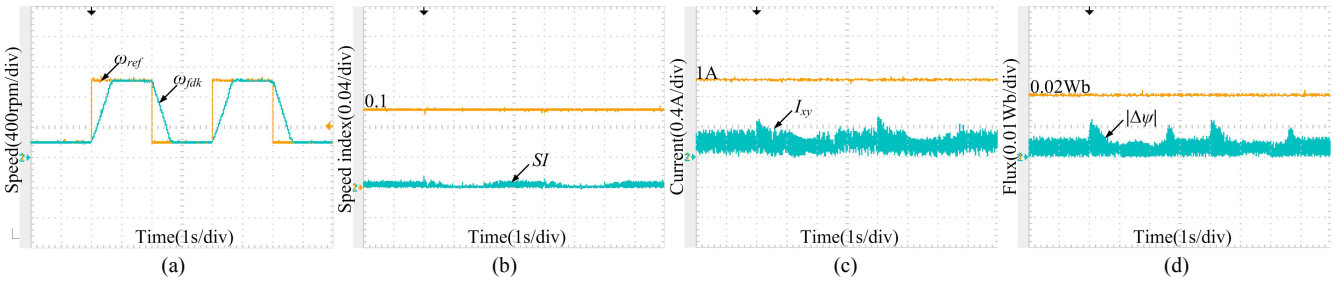

Fig. 8. Dynamic performance without fault: (a) speed; (b) diagnosis of speed sensor; (c) diagnosis of current on *x*-*y* subspace; (d) diagnosis of voltage sensor.

Fig. 9 shows the performance of fault diagnosis and tolerant control for speed-sensor fault. The given speed ω_{ref} is 1000rpm. During the operation, all the pulse signals from speed sensor (encoder) disappear. Because the feedback speed ω_{fdk} is calculated by the position change of latest 20ms, without fault-tolerant control, it will decrease to zero in 20ms in Fig. 9(a). Then, the speed PI controller is saturated consistently and the actual speed ω_{rl} increases to a maximum value limited by DC-link voltage. With the method in section IV-A, the estimated speed ω_{et} can track the real speed ω_{rl} precisely even under faulty state. As show in Fig. 9(b), it only takes about 2ms for the speed index *SI* to exceed its threshold 0.1 after fault. By using fault-tolerant control with the estimated speed, the speed is controlled stably in Fig. 9(c). In Fig. 9(d), Signal FL0 is presented to indicate whether the system remains normal state. It becomes 1 when a fault is detected. Signal FL1 and FL2 will act based on Table III, when the fault type is identified. T_{FO}, T_{FD} and T_{FT} represent the instants of occurrence, detection and identification of speed-sensor fault, respectively. The fault-tolerant control comes into effect at T_{FT}. Because the diagnostic method for speed-sensor fault is independent from the methods for other types of faults, T_{FD} and T_{FT} of the speed-sensor fault are with the same value. In Fig. 9(d), the values of Signal FL1 and FL2 are 0 and 1 respectively, which indicates that the detected fault is speed-sensor fault, according to Table III.

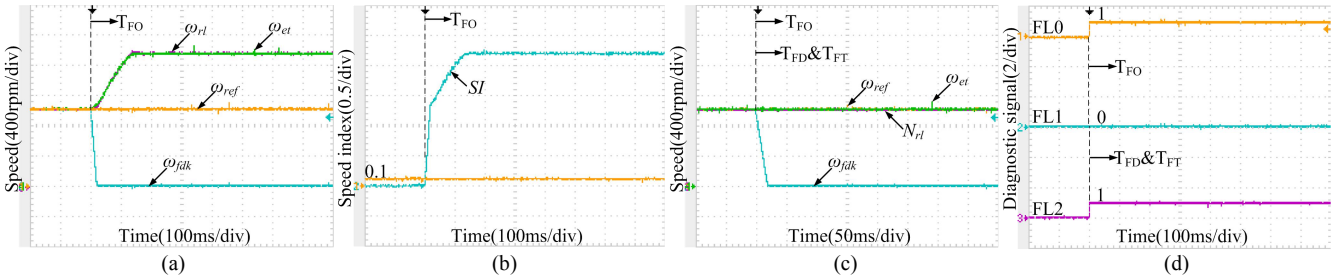

Fig. 9. Diagnostic and fault-tolerant process of speed-sensor fault: (a) speed without fault tolerance; (b) speed-sensor fault diagnosis; (c) speed with fault tolerance; (d) fault-location signal.

In this paper, the DC-link voltage-sensor fault is classified into two cases, according to the fault severity. The diagnosis of the first case of DC-link voltage-sensor fault is easy to implement. So, only the second case is considered in experiments

due to page limit. Fig. 10 shows the performance of fault diagnosis and fault-tolerant control for the second case of DC-link voltage-sensor fault. The error percentage of feedback voltage is set to increase uniformly from 0 to 20% in 200ms, as shown in Fig. 10(a). The estimated voltage U_{dc_et} is not calculated before the fault is identified. So, U_{dc_et} is set same as the feedback voltage U_{dc_fdk} before T_{FT}. After the voltage-sensor fault occurs, the absolute error of flux $|\Delta\psi|$ increases gradually and exceeds its threshold 0.02Wb at T_{FD}, as shown in Fig. 10(b). Fig. 10(c) shows the amplitude of feedback flux ψ_{fdk} and estimated flux ψ_{et}. Because the voltage model based stator flux ψ_{fdk} is used in the closed-loop control, it is still controlled around flux reference 0.02Wb after fault. On the other hand, the estimated flux ψ_{et} based on current model deviates from flux reference gradually. After the abnormal feature is detected at T_{FD}, it takes one fundamental period to determine the specific fault according to the feature of current I_{xy}. As shown in Fig. 10(d), I_{xy} does not exceed its own threshold 1A. The voltage-sensor fault is identified finally at T_{FT}, and the fault-tolerant operation is activated promptly. It can be observed that the voltage-sensor fault has not been misdiagnosed as other types of faults by observing current signal in Fig. 10(d) and speed index in Fig. 10(f). After fault-tolerant control is put into effect at T_{FT}, the estimated voltage U_{dc_et} replaces the feedback voltage U_{dc_fdk} to participate in system control. As shown in Fig. 10(a), the estimated voltage U_{dc_et} is almost same as the real voltage U_{dc_rl} and the absolute error of flux $|\Delta\psi|$ returns to low level.

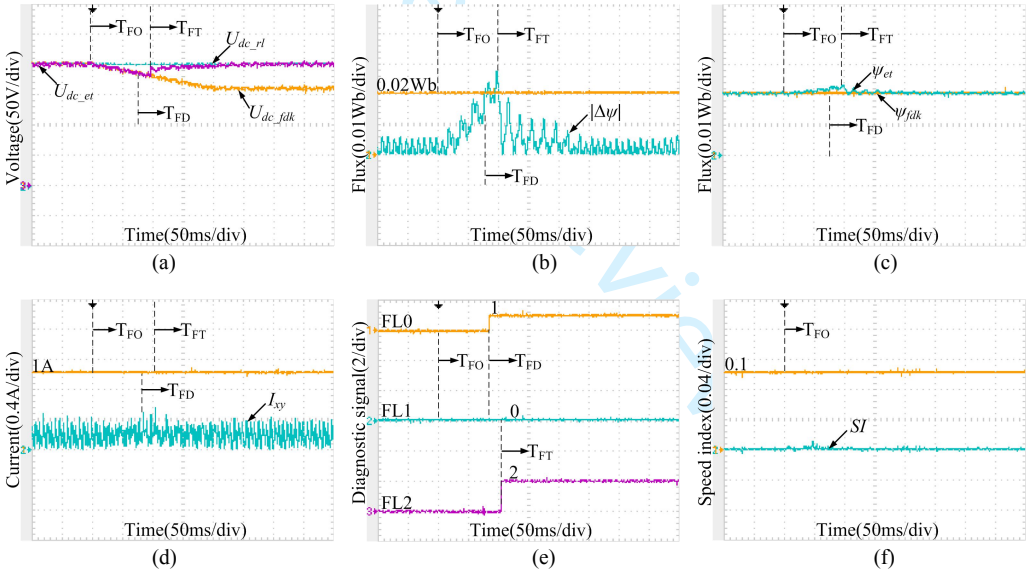

Fig. 10. Fault diagnosis and fault-tolerant control of DC-link voltage-sensor fault: (a) DC-link voltage; (b) diagnosis of voltage sensor; (c) amplitude of stator; (d) amplitude of current on harmonic subspace; (e) fault-location signal; (f) speed index.

Fig. 11 shows the performance of fault diagnosis and fault-tolerant control for open-circuit fault in phase-A. After the fault occurs, the phase currents become abnormal, as show in Fig. 11(a) and Fig. 11(b). The amplitude of current on *x*-*y* subspace I_{xy} exceeds its threshold 1A and the fault is detected at T_{FO} immediately in Fig. 11(c). Then, it will take one fundamental period to identify the specific fault. As shown in Fig. 11(d), the measured current trajectory on *x*-*y* subspace under faulty state coincides with the expected result in Fig. 4. With the second step of three-step diagnostic method in section IV-C, i_{y1} is determined to be the minimum value of six average absolute currents, which are Fig. 11(e), Fig. 11(f) and Fig. 11(g). Therefore, the current trajectory on *x*-*y* subspace moves along x_1 axis, which is perpendicular to y_1 axis. With

Table I, three possible faults are O_A, S_{A1} and S_{A2}. According to Fig. 11(h) and Fig. 11(i), both CI_{A+} and CI_{A-} are smaller than their threshold 0.5. So, the open-phase fault is detected at T_{FD}, and identified and tolerated at T_{FT} , as shown in Fig. 11(j). Fig. 11(k) verifies that open-phase fault will not be misdiagnosed as speed-sensor fault. By adopting voltage compensation based fault-tolerant control at T_{FT}, the torque ripple disappears in Fig. 11(l).

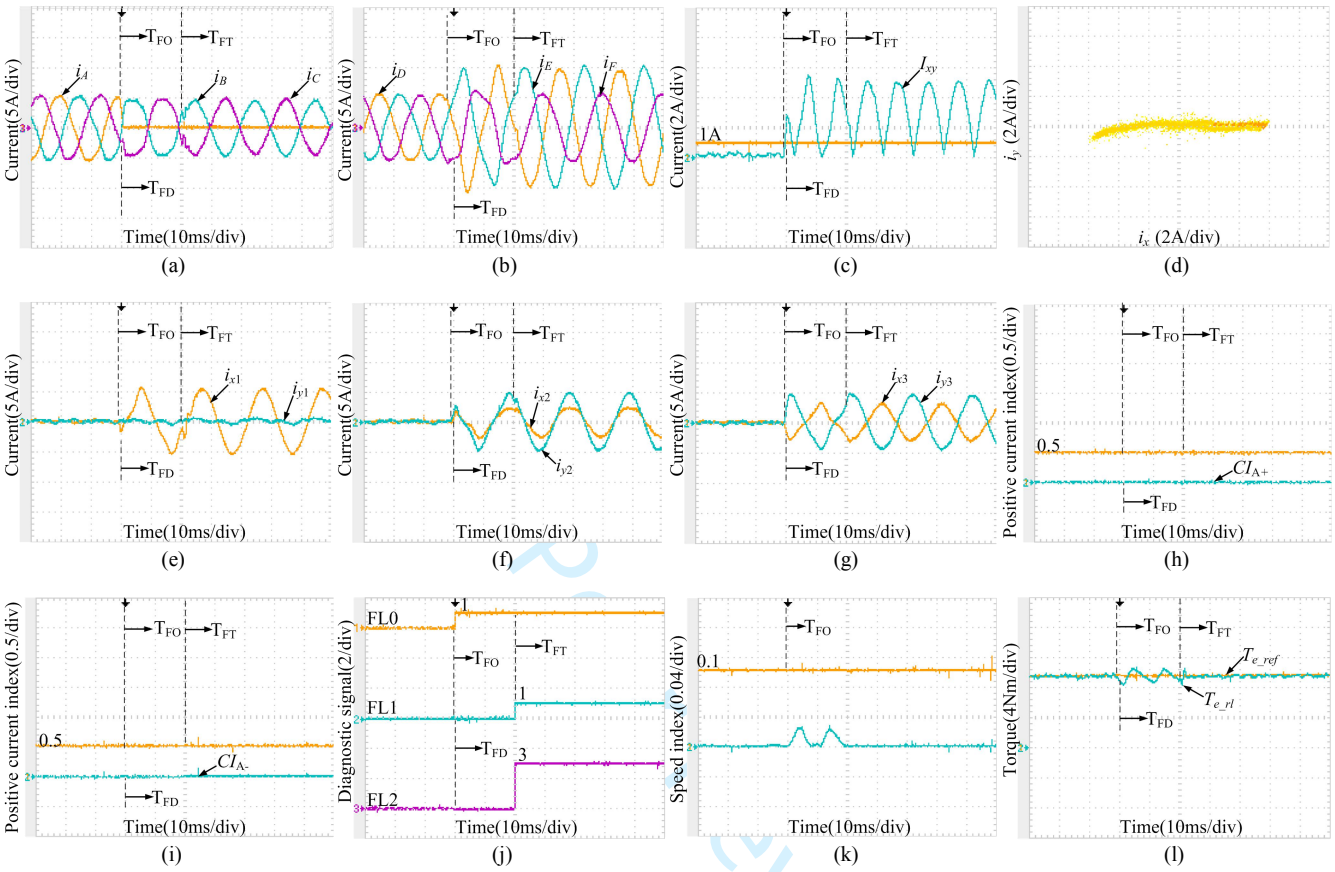

Fig. 11. Fault diagnosis and fault-tolerant process of open-circuit fault in phase-A: (a) phase currents of ABC; (b) phase currents of DEF; (c) amplitude of current on harmonic subspace; (d) current trajectory on harmonic subspace; (e) currents on x_1 axis and y_1 axis; (f) currents on x_2 axis and y_2 axis; (g) currents on x_3 axis and y_3 axis; (h) positive current index; (i) negative current index; (j) fault-location signal; (k) speed index; (l) torque.

Fig. 12 shows the performance of fault diagnosis and fault-tolerant control for S_1 open-switch fault in phase-A. After fault occurs, the phase currents become abnormal, as show in Fig. 12(a) and Fig. 12(b). The current I_{xy} exceeds its threshold 1A and the fault is detected at T_{FO} immediately in Fig. 12(c). Then, it takes one fundamental period to identify the specific fault. The slope of current trajectory on *x*-*y* subspace under faulty state in Fig. 12(d) agrees with the result in Fig. 4. According to the second step of three-step diagnostic method, i_{y1} is the minimum one of six average absolute currents, as show in Fig. 12(e), Fig. 12(f) and Fig. 12(g). Therefore, the current trajectory on *x*-*y* subspace moves along i_{x1} axis. With Table I, three fault possibilities are O_A, S_{A1} and S_{A2}. As shown in Fig. 12(h) and Fig. 12(i), CI_{A+} is larger than it threshold 0.5 and CI_{A-} is smaller than its threshold 0.5. So, the S_1 open-switch fault in phase-A is finally identified at T_{FT}. Fig. 12(j) shows that the fault is detected at T_{FD}, and identified and tolerated at T_{FT}. Fig. 12(k) shows that open-phase fault will not be misdiagnosed as other types of faults such as the speed-sensor fault. By using fault-tolerant control, the torque ripple caused by open-switch fault is mitigated effectively, as shown in Fig. 12(l).

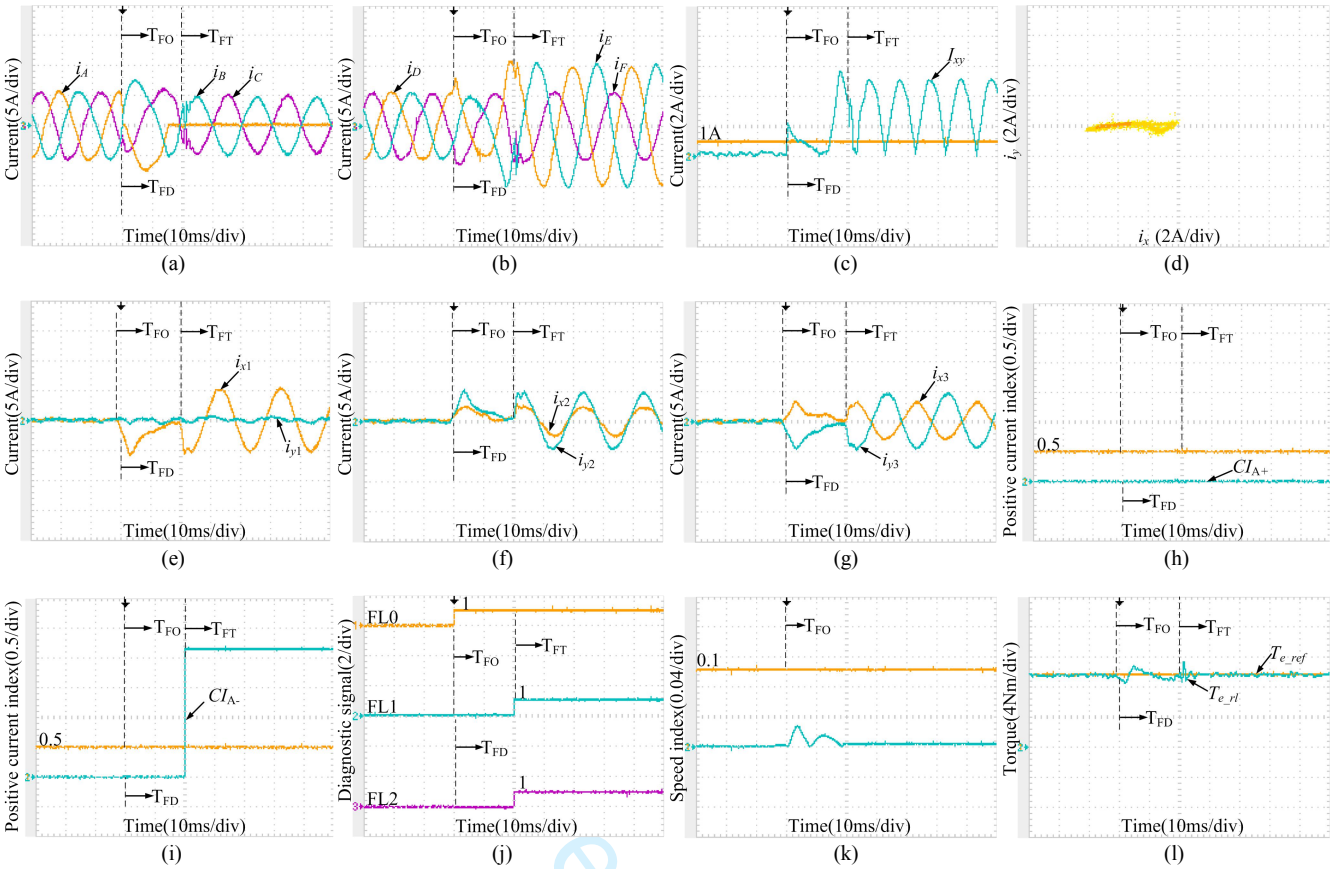

Fig. 12. Fault diagnosis and fault-tolerant control of switch S_{A1} fault: (a) phase currents of ABC; (b) phase currents of DEF; (c) amplitude of current on harmonic subspace; (d) current trajectory on harmonic subspace; (e) currents on x_1 axis and y_1 axis; (f) currents on x_2 axis and y_2 axis; (g) currents on x_3 axis and y_3 axis; (h) positive current index; (i) negative current index; (j) fault-location signal; (k) speed index; (l) torque.

Fig. 13 shows the performance of fault diagnosis and fault-tolerant control for current-sensor fault in phase-A. A worst case of current-sensor fault is considered. The feedback value of current sensor in phase-A is forced to be zero at T_{FO}. After fault occurs, the phase currents become asymmetric, as show in Fig. 13(a) and Fig. 13(b). The amplitude of current on *x-y* subspace I_{xy} exceeds its threshold 1A and the fault is detected immediately in Fig. 13(c). Then, it will take one fundamental period to identify the specific fault. The current trajectory on *x-y* subspace under faulty state in Fig. 13(d) is same as the expected result in Fig. 3. According to the second step of three-step diagnostic method, i_{x3} is the minimum one of six average absolute currents, as show in Fig. 13(e), Fig. 13(f) and Fig. 13(g). Therefore, the current trajectory on *x-y* subspace moves along i_{y3} axis. With Table I, four fault possibilities are O_D, S_{D1}, S_{D2} and C_A. Because both CI_{D+} and CI_{D-} are larger than their threshold values of 0.5, the current-sensor fault in phase-A is finally identified at T_{FT}, as shown in Fig. 13(h) and Fig. 13(i). Fig. 13(j) shows that the fault is detected at T_{FD}, then identified and tolerated at T_{FT}. Fig. 13(k) shows that current-sensor fault will not be misdiagnosed as other types of faults such as the speed-sensor fault. After using fault-tolerant control at T_{FT}, the incorrect phase-A current are replaced by the estimated one. The currents on each coordinate system returns to normal and the torque becomes stable, as shown in Fig. 13(l).

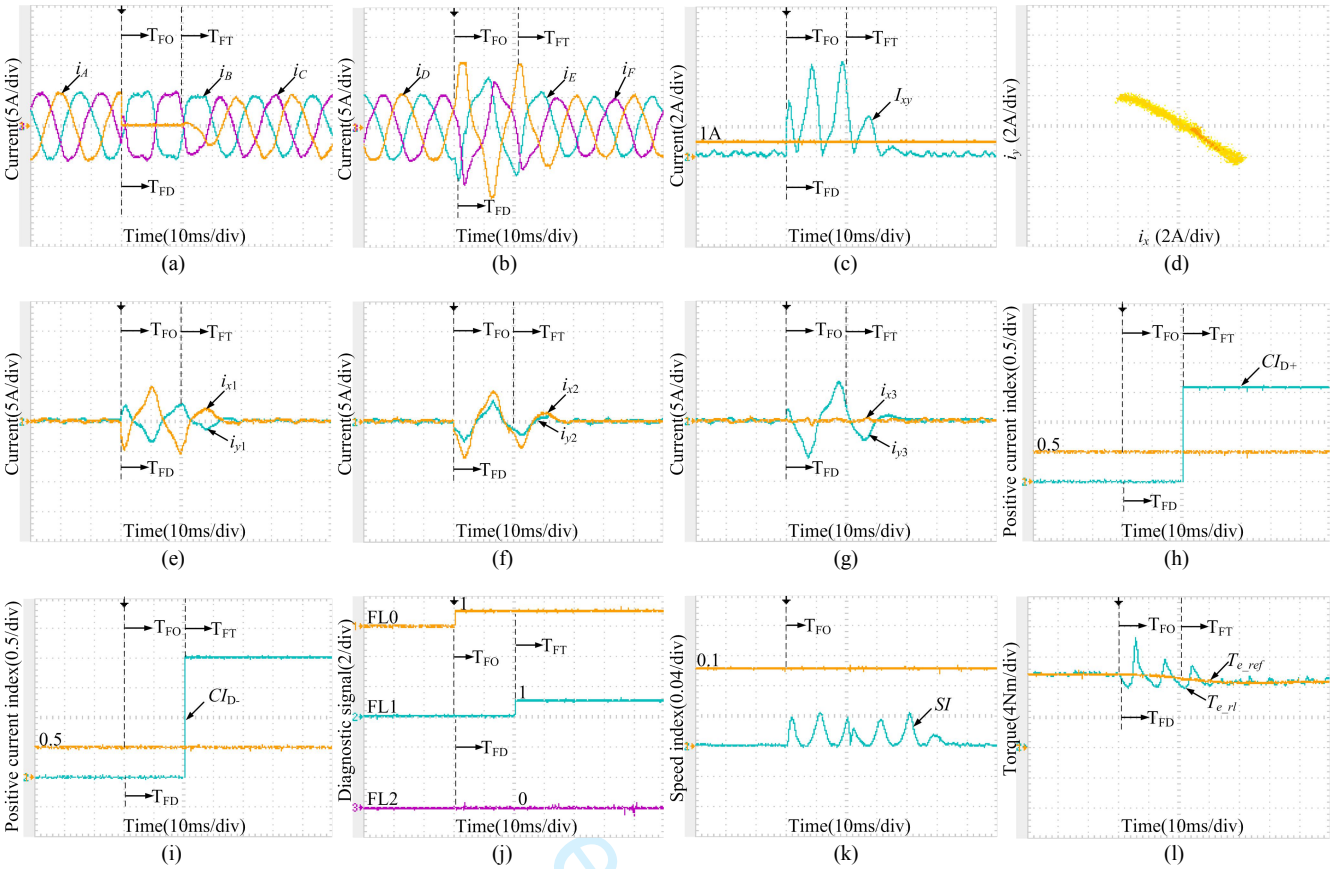

Fig. 13. Fault diagnostic and fault-tolerant control of current sensor fault in phase-A: (a) phase currents of ABC; (b) phase currents of DEF; (c) amplitude of current on harmonic subspace; (d) current trajectory on harmonic subspace; (e) currents on x_1 axis and y_1 axis; (f) currents on x_2 axis and y_2 axis; (g) currents on x_3 axis and y_3 axis; (h) positive current index; (i) negative current index; (j) fault-location signal; (k) speed index; (l) torque.

VI. CONCLUSIONS

In this paper, a comprehensive study is presented for fault diagnosis and tolerance of dual-three phase PMSM drives. A SVM based DTC is applied for the basic control frame. Based on this framework, fault diagnostic and tolerant methods have been proposed for five types of faults (speed-sensor fault, voltage-sensor fault, current-sensor fault, open-phase fault and open-switch fault). Firstly, the speed-sensor fault is diagnosed and tolerated by approximately estimating the rotor angle speed to be the rotating speed of stator flux. Secondly, the current model based stator flux observer is combined with the voltage model based stator flux observer to achieve the diagnosis and tolerance of DC-link voltage-sensor fault. Thirdly, a three-step method is designed to diagnose three types of faults related to current signals, namely current-sensor fault, open-phase fault and open-switch fault simultaneously. Especially, a VSD based current estimation method is proposed to achieve fault-tolerant control for current-sensor faults. Both open-phase fault and open-switch fault have been tolerated by using a voltage compensation based fault-tolerant control. No additional hardware is required to achieve the proposed fault-diagnosis and fault-tolerant schemes. The experimental results have been given to verify the effectiveness of the proposed schemes.

REFERENCES

[1] E. Levi, F. Barrero and M. J. Duran, "Multiphase machines and drives—revisited," *IEEE Trans. Ind. Electron*, vol. 63, no. 1, pp. 429-432, Jan. 2016.

[2] M.Mengoni, L. Zarri, A. Tani, L. Parsa, G. Serra, and D. Casadei, "High-torque-density control of multiphase induction motor drives operating over a wide speed range," *IEEE Trans. Ind. Electron.*, vol. 62, no. 2, pp. 814-825, Feb. 2015.

[3] W. N. W. A. Munim, M. J. Duran, H. S. Che, M. Bermúdez, I. González-Prieto and N. A. Rahim, "A unified analysis of the fault tolerance capability in six-phase induction motor drives," *EEE Trans. Ind. Electron.*, vol. 32, no. 10, pp. 7824-7836, Oct. 2017.

[4] L. De Lillo, L. Empringham, P. W. Wheeler, S. Khwan-On, and C. Gerada, "Multiphase power converter drive for fault-tolerant machine development in aerospace applications," *IEEE Trans. Ind. Electron.*, vol. 57, pp. 575-583, Feb. 2010.

[5] F. Mwasilu and J. W. Jung, "Enhanced fault-tolerant control of interior PMSMs based on an adaptive EKF for EV traction applications," *IEEE Trans. Ind. Electron.*, vol. 31, no. 8, pp. 5746-5758, Aug. 2016.

[6] A. Bellini, F. Filippetti, C. Tassoni and G. A. Capolino, "Advances in diagnostic techniques for induction machines," *IEEE Trans. Ind. Electron.*, vol. 55, no. 12, pp. 4109-4126, Dec. 2008.

[7] T. A. Najafabadi, F. R. Salmasi and P. Jabehdar-Maralani, "Detection and isolation of speed-, DC-link voltage-, and current-sensor faults based on an adaptive observer in induction-motor drives," *IEEE Trans. Ind. Electron.*, vol. 58, no. 5, pp. 1662-1672, May 2011.

[8] S. Nandi, H. A. Toliyat and X. Li, "Condition monitoring and fault diagnosis of electrical motors-a review," *IEEE Trans. Energy Convers.*, vol. 20, no. 4, pp. 719-729, Dec. 2005.

[9] Z. Wang, X. Shi, L. M. Tolbert, F. Wang and B. J. Blalock, "A di/dt Feedback-Based Active Gate Driver for Smart Switching and Fast Overcurrent Protection of IGBT Modules," *IEEE Trans. Power. Electron..*, vol. 29, no. 7, pp. 3720-3732, July 2014.

[10] W. Zhang, D. Xu, P. N. Enjeti, H. Li, J. T. Hawke and H. S. Krishnamoorthy, "Survey on fault-tolerant techniques for power electronic converters," *IEEE Trans. Power. Electron.*, vol. 29, no. 12, pp. 6319-6331, Dec. 2014.

[11] Y. Yu, Y. Zhao, B. Wang, X. Huang and D. Xu, "Current Sensor Fault Diagnosis and Tolerant Control for VSI-Based Induction Motor Drives," *IEEE Trans. Power. Electron.* vol. 33, no. 5, pp. 4238-4248, May 2018.

[12] B. Cai, Y. Zhao, H. Liu and M. Xie, "A Data-Driven Fault Diagnosis Methodology in Three-Phase Inverters for PMSM Drive Systems," *IEEE Trans. Power. Electron.* vol. 32, no. 7, pp. 5590-5600, July 2017.

[13] G. H. B. Foo, X. Zhang and D. M. Vilathgamuwa, "A sensor fault Detection and Isolation Method in Interior Permanent-Magnet synchronous motor drives based on an extended Kalman filter," *IEEE Trans. Ind. Electron.*, vol. 60, no. 8, pp. 3485-3495, Aug. 2013.

[14] M. Salehifar, R. Salehi Arashloo, M. Moreno-Eguilaz, V. Sala and L. Romeral, "Observer-based open transistor fault diagnosis and fault-tolerant control of five-phase permanent magnet motor drive for application in electric vehicles," *IET Power Electron.* vol. 8, no. 1, pp. 76-87, Jan. 2015.

[15] F. R. Salmasi, "A self-healing induction motor drive with model free sensor tampering and sensor fault detection, isolation, and compensation," *IEEE Trans. Ind. Electron.*, vol. 64, no. 8, pp. 6105-6115, Aug. 2017.

[16] H. Berriri, M. W. Naouar and I. Slama-Belkhodja, "Easy and fast sensor fault detection and isolation algorithm for electrical drives," *IEEE Trans. Power. Electron..*, vol. 27, no. 2, pp. 490-499, Feb. 2012.

[17] M. J. Duran, I. Gonzalez-Prieto, N. Rios-Garcia and F. Barrero, "A simple, fast, and robust open-phase fault detection technique for six-phase induction motor drives," *IEEE Trans. Power. Electron..*, vol. 33, no. 1, pp. 547-557, Jan. 2018

[18] A. Arafat, S. Choi and J. Baek, "Open-phase fault detection of a five-phase permanent magnet assisted synchronous reluctance motor based on symmetrical components theory," *IEEE Trans. Ind. Electron.*, vol. 64, no. 8, pp. 6465-6474, Aug. 2017.

[19] M. Trabelsi, N. K. Nguyen and E. Semail, "Real-time switches fault diagnosis based on typical operating characteristics of five-phase permanent-magnetic synchronous machines," *IEEE Trans. Ind. Electron.*, vol. 63, no. 8, pp. 4683-4694, Aug. 2016.

[20] C. Chakraborty and V. Verma, "Speed and current sensor fault detection and isolation technique for induction motor drive using axes transformation," *IEEE Trans. Ind. Electron.*, vol. 62, no. 3, pp. 1943-1954, Mar. 2015.

[21] G. F. H. Beng, X. Zhang and D. M. Vilathgamuwa, "Sensor fault-resilient control of interior permanent-magnet synchronous motor drives," *IEEE Trans.* Mechatron., vol. 20, no. 2, pp. 855-864, April 2015.

[22] W. Wang, J. Zhang and M. Cheng, "Common model predictive control for permanent-magnet synchronous machine drives considering single-phase open-circuit fault," *IEEE Trans. Power. Electron..*, vol. 32, no. 7, pp. 5862-5872, July 2017.

[23] M. Bermudez, I. Gonzalez-Prieto, F. Barrero and H. Guzman, "Open-phase fault tolerant direct torque control technique for five-phase induction motor drives," *IEEE Trans. Ind. Electron.*, vol. 64, no. 2, pp. 902-911, Feb 2017.

[24] W. N. W. A. Munim, M. J. Duran, H. S. Che, M. Bermúdez, I. González-Prieto and N. A. Rahim, "A unified analysis of the fault tolerance capability in six-phase induction motor drives," *IEEE Trans. Power. Electron.*, vol. 32, no. 10, pp. 7824-7836, Oct. 2017.

[25] B. Mirafzal, "Survey of fault-tolerance techniques for three-phase voltage source inverters," *IEEE Trans. Ind. Electron.*, vol. 61, no. 10, pp. 5192-5202, Oct. 2014.

[26] X. Wang, Z. Wang, M. Cheng, and Y. Hu, "Remedial strategies of T-NPC three-level asymmetric six-phase PMSM drives based on SVM-DTC", *IEEE Trans. Ind. Electron*, vol. 64, no. 9, pp. 6841-6853, Sept. 2017.

[27] Y. Zhao and T.A. Lipo, "Space vector PWM control of dual three-phase induction machine using vector space decomposition," *IEEE Trans. Ind. Appl.*, vol. 31, no. 5, pp. 1100-1109, Sept./Oct. 1995.

[28] X. Wang, Z. Wang, J. Chen, M. Cheng, L. Xu, "Direct torque control of dual three-phase PMSM drives based on two-step voltage vector synthesis SVM," *IEEE International Power Electronics and Motion Control Conference* (IPEMC-ECCE Asia), pp. 641-647, July 2016, Hefei, China

[29] L. Parsa and H. A. Toliyat, "Sensorless direct torque control of five-phase interior permanent-magnet motor drives," *IEEE Trans. Ind. Appl.*, vol. 43, no. 4, pp. 952-959, July/aug. 2007.

[30] D. Swierczynski, M. P. Kazmierkowski, and F. Blaabjerg, "DSP based direct torque control of permanent magnet synchronous motor (PMSM) using space vector modulation (SVM-DTC)," *International Symposium on Industrial Electronics*, 2002, pp. 723-727.